A Mechanical Sensorless Vector-Controlled Induction Motor System with Parameter Identification by the Aid of Image Processor

Mineo Tsuji*, Shuo Chen† , Tatsunori Motoo*, Yuki Kawabe* and Shin-ichi Hamasaki*

Abstract - This paper presents a mechanical sensorless vector-controlled system with parameter identification by the aid of image processor. Based on the flux observer and the model reference adaptive system method, the proposed sensorless system includes rotor speed estimation and stator resistance identification using flux errors. Since the mathematical model of this system is constructed in a synchronously rotating reference frame, a linear model is easily derived for analyzing the system stability, including motor operating state and parameter variations. Because it is difficult to identify rotor resistance simultaneously while estimating rotor speed, a low-accuracy image processor is used to measure the mechanical axis position for calculating the rotor speed at a steady-state operation. The rotor resistance is identified by the error between the estimated speed using the estimated flux and the calculated speed using the image processor. Finally, the validity of this proposed system has been proven through experimentation.

Keywords: Induction motor, vector control, parameter identification, image processing

1. Introduction

In a vector-controlled induction motor (IM) drive, accurate knowledge of the machine parameters is required to ensure correct alignment of the stator current vector to the rotor flux vector, to decouple the flux- and torque-producing current and to tune the current control loops [1]-[3]. A speed sensor is usually requisite for vector control. In practical applications, the use of speed sensor does have many problems, especially in hostile environments. Vector-controlled induction motor drives without speed sensor have become an attractive and commercially expanding technology in the past years [4-5]. In a speed sensorless vector control system, it is difficult to identify rotor resistance and estimate rotor speed simultaneously. However, the actual speed has been greatly influenced by the rotor resistance being varied with the inner temperature of IM. It is necessary to obtain the actual value of rotor resistance for torque and speed control accuracy.

On the other hand, with the rapid development of semiconductor and microprocessor technology, image processing technology has been widely used in industrial applications, such as factory automation system and industrial robot. The advantages of image process are flexibility and non-touched measurement. Charge-coupled device (CCD) image sensor has advantages of small size, high reliability and low cost. It is easy to mount a CCD image sensor on the robot arm or front end of manipulator or other requisite place for monitoring and regulating. In general, the response of image processing is slow because a long processing time is requisite and the information obtained from image processing has not high accuracy. So it is difficult to replace the mechanical position sensor with image processor in servo system. Our purpose is to develop a high-performance adjustable-speed system using vector-controlled induction motor drive replacing the mechanical speed sensor with an image processor. In this paper, we introduce a speed sensorless vector-controlled induction motor system. Based on the flux observer and the model reference adaptive system (MRAS) method, this system includes a rotor speed estimator and stator resistance identifier using flux errors [6]. Since the mathematical model of this system is constructed in a synchronously rotating reference frame, a linear model is easily derived for analyzing the system stability, including motor operating state and parameter variations. This system can work in motoring and regenerating modes. The adjustable-speed range is around 1:200. The advantages are simplicity and avoidance of problems caused by using only a voltage model. Because it is difficult to identify rotor resistance simultaneously while estimating rotor speed, we use a low-accuracy image processor to measure the me-

This paper was received the best paper award from ICEMS 2005, which held in Nanjing, China from Sep. 27 to Sep. 29, 2005

† Corresponding Author: Department of Electrical & Electornic Engineering, Faculty of Engineering, Nagasaki University 1-14, Bunkyou-machi, Nagasaki 852-8521, JAPAN (shuochen@net.nagasaki-u.ac.jp)

* Department of Electrical & Electornic Engineering, Faculty of Engineering, Nagasaki University 1-14, Bunkyou- machi, Nagasaki 852-8521, JAPAN

Received November 3, 2005 ; Accepted November 17, 2005

chanical axis position for calculating the rotor speed at a steady-state operation. The rotor resistance is identified by the error between the estimated speed using the estimated flux and the calculated speed using the image processor. Finally, the effectiveness of this proposed system is verified by experimentation.

2. Proposed System

The proposed system shown in Fig. 1 includes three parts. The first part is a speed sensorless vector-controlled system of speed estimator and stator resistance identifier. The second is a speed calculator by the aid of image processor. The third is a rotor resistance identifier by using speed error.

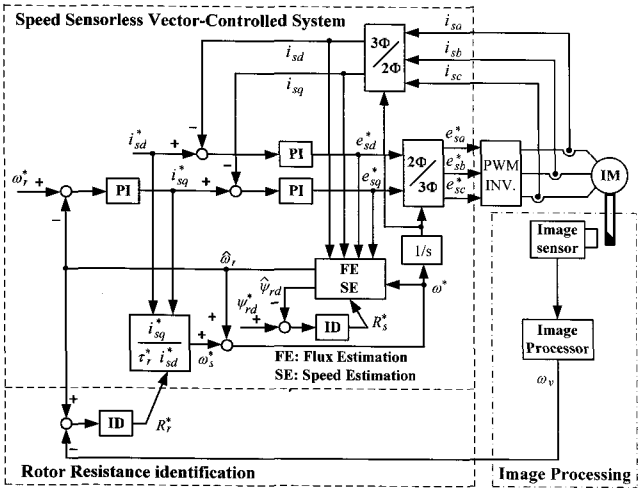

Fig. 1 Block diagram of the proposed system

2.1 Speed Estimation and Stator Resistance Identification

An induction motor can be described by the following equations in an arbitrary reference frame [7]:

voltage model

$$e_{sd} = (R_s + \sigma L_s p) i_{sd} - \omega \sigma L_s i_{sq} + \frac{M}{L_r} p\psi_{rd} - \frac{M}{L_r} \omega \psi_{rq} \quad (1)$$

$$e_{sq} = \omega \sigma L_s i_{sd} + (R_s + \sigma L_s p) i_{sq} + \frac{M}{L_r} \omega \psi_{rd} + \frac{M}{L_r} p\psi_{rq} \quad (2)$$

current model

$$0 = -\frac{1}{\tau_r} M i_{sd} + (\frac{1}{\tau_r} + p)\ \psi_{rd} - (\omega - \omega_r)\ \psi_{rq} \quad (3)$$

$$0 = -\frac{1}{\tau_r} M i_{sq} + (\omega - \omega_r)\ \psi_{rd} + (\frac{1}{\tau_r} + p)\ \psi_{rq} \quad (4)$$

where $\sigma = 1 - M^2/(L_s L_r)$, $\tau_r = L_r/R_r$, $p = d/dt$.

In this paper, a d-q synchronously rotating reference frame with respect to the rotor flux computed by the current model is chosen. So, the q-axis flux ψ_{rq}^{C} of this model is zero. Letting the reference maganetizing current i_{sd}^{*} be constant, (3) and (4) can be rewritten as

$$\psi_{rd}^{C} = M i_{sd}^{*} \quad (5)$$

$$p\theta^{*} = \omega^{*} = \hat{\omega}_r + \frac{i_{sq}^{*}}{\tau_r^{*} i_{sd}^{*}} \quad (6)$$

where $\hat{\omega}_r$ is the estimated rotor speed and the superscript "$*$" denotes the controller's variables.

To estimate the fluxes from the voltage model of (1) and (2), an integrating process is needed. However, it is difficult to maintain the system stability of a pure integrator due to motor parameter variation. In order to overcome this problem, the voltage model is modified by the current model from the viewpoint of the observer theory as follows [6]:

$$p\psi_{rd}^{V} = \frac{L_r}{M}\{e_{sd}^{*} - (R_s^{*} + \sigma L_s p)\ i_{sd} + \omega^{*} \sigma L_s\ i_{sq}\} + \omega^{*} \psi_{rq}^{V} + \frac{\psi_{rd}^{C} - \psi_{rd}^{V}}{T_c} \quad (7)$$

$$p\psi_{rq}^{V} = \frac{L_r}{M}\{e_{sq}^{*} - (R_s^{*} + \sigma L_s p)\ i_{sq} - \omega^{*} \sigma L_s\ i_{sd}\} - \omega^{*} \psi_{rd}^{V} + \frac{\psi_{rq}^{C} - \psi_{rq}^{V}}{T_c} \quad (8)$$

where T_c is the reciprocal of the flux observer gain.

The estimated q-axis rotor flux ψ_{rq}^{V} computed by (8) should be zero because ψ_{rq}^{V} must be equal to ψ_{rq}^{C} (= 0) when the estimated speed is correct. According the MRAS theory, the rotor speed can be estimated by

$$\hat{\omega}_r = K_\omega\ (1 + \frac{1}{T_\omega p})\ \psi_{rq}^{V}. \quad (9)$$

In the above equation, ψ_{rq}^{V} must converge to zero by proportional plus integral (PI) regulator. The d-axis flux error between the the adjustable model (votage model) and

the reference model (current model) can be considered to be caused by the stator resistance variation. By analyzing the flux error at a steady-state operation, a stator resistance identificaion algorithm using the *d*-axis flux error can be expressed as

$$pR_s^* = \text{sign}(\omega^* i_{sq}^*)\,\mu_s\,(\psi_{rd}^V - \psi_{rd}^C) \tag{10}$$

where μ_s is the identification gain. $\text{sign}(\omega^* i_{sq}^*)$ is +1 in motoring mode and -1 in regenerating mode. The stator resistance identification and the speed estimation can be achieved simultaneously.

2.2 Speed Calculation by Image Processor

Fig. 2 shows the image processing configuration. A commercial image sensor (CCD camera) is used to take a picture of the white-black mark stuck on the motor axis, as shown in Fig. 3. After decoding and binary processing, the axis position can be calculated by the proportion of white-dot amount and black-dot amount in one picture. If the axis position is $\theta(k-1)$ at a moment and $\theta(k)$ after a period of *T*, the rotor speed can be calculated by

$$\omega_v = \frac{\theta(k)-\theta(k-1)}{T}. \tag{11}$$

Here ω_v means the calculated speed by using the image processor. As the position calculator output is only 4 bit, 1-bit change presents that the axis rotates 22.5 degrees. Though the detecting accuracy is very poor, it can be improved by a relatively long period, compared with the sampling period of the overall system. Therefore, this calculated speed can be only used at a steady-state operation.

2.3 Rotor Resistance Identification

In (6), the angular velocity ω^* is modified by the speed sensorless vector-controlled system and must be constant at a steady state. So (6) can be rewritten

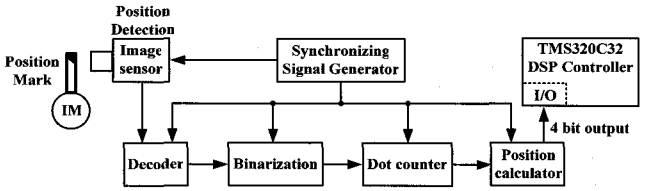

Fig. 2 Image processing configuration

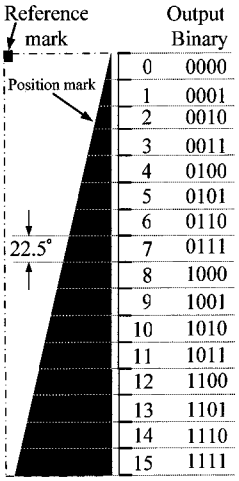

Fig. 3 Position mark and output

$$\omega^* = \hat{\omega}_r + \frac{R_r^*}{L_r i_{sd}^*} i_{sq}^* \tag{12}$$

where R_r^* is the controller's value of rotor resistance. In this system, $\hat{\omega}_r$ is estimated by (9) and the error between $\hat{\omega}_r$ and ω_r^* (speed command) is used to modify the torque-producing current by PI regulator. Therefore, $\hat{\omega}_r$ must be converged to ω_r^* whether the actual values of stator and rotor resistances vary. Using (10), the stator resistance can be identified and would not influence the flux estimation. The error between $\hat{\omega}_r$ and the actual speed ω_r can be considered to be caused by the rotor resistance variation and increases with load raising. Since the calculated speed ω_v is equal to ω_r and the current control is ideal at a steady state, (4) can be rewritten as

$$\omega^* = \omega_v + \frac{R_r}{L_r i_{sd}^*} i_{sq}^*. \tag{13}$$

where R_r is the actual value of rotor resistance. From (12) and (13), the following equation can be obtained:

$$R_r - R_r^* = \frac{i_{sd}^* L_r}{i_{sq}^*}(\hat{\omega}_r - \omega_v). \tag{14}$$

(14) shows that $\omega_v < \hat{\omega}_r$ if $R_r > R_r^*$ while operating at $i_{sq}^* > 0$. In contrast, $\omega_v > \hat{\omega}_r$ if $R_r > R_r^*$ while operating at $i_{sq}^* < 0$. Therefore, an identification algorithm of rotor resistance identification using the error between ω_v and $\hat{\omega}_r$ is proposed as follows:

$$pR_r^* = \text{sign}\left(i_{sq}^*\right)\mu_r\left(\hat{\omega}_r - \omega_v\right) \tag{15}$$

where μ_r is the identification gain of rotor resistance. $\text{sign}\left(i_{sq}^*\right)$ is +1 when $i_{sq}^* > 0$, and -1 when $i_{sq}^* < 0$.

3. Stability Analysis

The stability analysis of the proposed system shown in Fig.1 is presented. By taking a small perturbation at a steady-state operating point, a linear model of the proposed system can be deduced. To simplify the analysis, the following assumptions are considered.

1) The motor have those nominal values except for the stator and rotor resistances.
2) The motor actual voltages are equal to the voltages' commands and the *d-q* synchronously rotating reference frame is chosen, the *d-q* voltages are given by

$$e_{sd} = e_{sd}^*,\ e_{sq} = e_{sq}^*. \tag{16}$$

The induction motor can be described by (1)-(4) and the equation of motion [8]. By using these equations, the linear model of the motor can be derived as follow:

$$p\Delta \boldsymbol{x}_s = \boldsymbol{A}_s\Delta \boldsymbol{x}_s + \boldsymbol{B}_s\Delta \boldsymbol{u}_s + \boldsymbol{B}_l\Delta T_L \tag{17}$$

where

$$\Delta \boldsymbol{x}_s = \left[\Delta i_{sd}\ \ \Delta i_{sq}\ \ \Delta \psi_{rd}\ \ \Delta \psi_{rq}\ \ \Delta \omega_r\right]^T$$
$$\Delta \boldsymbol{u}_s = \left[\Delta e_{sd}^*\ \ \Delta e_{sq}^*\ \ \Delta \omega^*\right]^T$$

Here T_L is the load torque. The linear model of the controller is expressed is

$$p\Delta \boldsymbol{z} = \boldsymbol{A}_x\Delta \boldsymbol{x}_s + \boldsymbol{A}_z\Delta \boldsymbol{z} + \boldsymbol{B}_z\Delta \boldsymbol{u}_s + \boldsymbol{B}_r\Delta \omega_r^* \tag{18}$$

$$\Delta \boldsymbol{u}_s = \boldsymbol{F}_x\Delta \boldsymbol{x}_s + \boldsymbol{F}_z\Delta \boldsymbol{z} + \boldsymbol{F}_r\Delta \omega_r^* \tag{19}$$

where

$$\Delta \boldsymbol{z} = \left[\Delta e_\omega\ \ \Delta e_s\ \ \Delta e_{vd}\ \ \Delta e_{vq}\ \ \Delta \psi_{sd}^v\ \ \Delta \psi_{sq}^v\right]^T.$$

Here, Δe_ω, Δe_s, Δe_{vd}, and Δe_{vq} are produced by PI regulators for speed estimation, speed control, and current control, respectively. From (17)-(19), the linear model of the whole system can be written as follows:

$$p\Delta \boldsymbol{x} = \boldsymbol{A}\Delta \boldsymbol{x} + \boldsymbol{B}\Delta \boldsymbol{u} + \boldsymbol{B}_L\Delta T_L \tag{20}$$

where

$$\Delta \boldsymbol{x} = \left[\Delta \boldsymbol{x}_s^T\ \ \Delta \boldsymbol{z}^T\right]^T$$
$$\boldsymbol{A} = \begin{bmatrix} \boldsymbol{A}_s + \boldsymbol{B}_s\boldsymbol{F}_x & \boldsymbol{B}_s\boldsymbol{F}_z \\ \boldsymbol{A}_x + \boldsymbol{B}_z\boldsymbol{F}_x & \boldsymbol{A}_z + \boldsymbol{B}_z\boldsymbol{F}_x \end{bmatrix}$$
$$\boldsymbol{B} = \begin{bmatrix} \boldsymbol{B}_s\boldsymbol{F}_r \\ \boldsymbol{B}_z\boldsymbol{F}_r + \boldsymbol{B}_r \end{bmatrix},\ \boldsymbol{B}_L = \begin{bmatrix} \boldsymbol{B}_l \\ \boldsymbol{0} \end{bmatrix}.$$

The output equation and the speed transfer function derived from the above linear equations can be given by

$$\Delta \omega_r = \boldsymbol{C}\Delta \boldsymbol{x} \tag{21}$$

$$G(s) = \frac{\Delta \omega_r}{\Delta \omega_r^*} = \frac{\boldsymbol{C}\text{adj}(s\boldsymbol{I} - \boldsymbol{A})\boldsymbol{B}}{|s\boldsymbol{I} - \boldsymbol{A}|}. \tag{22}$$

where

$$\boldsymbol{C} = \left[0\ \ 0\ \ 0\ \ 0\ \ 1\ \ 0\ \ 0\ \ 0\ \ 0\ \ 0\ \ 0\right].$$

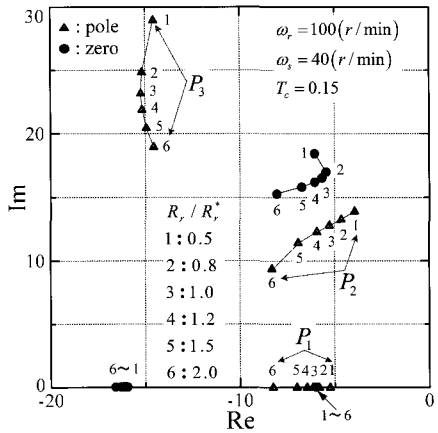

Fig. 4 Trajectories of poles and zeros with R_r change (In motoring mode)

Fig. 4 shows the root trajectories of the poles and zeros on the *s* plane calculated from (22) in which R_r is changed from $0.5R_{ro}$ to $2.0R_{ro}$, and R_{ro} is the nominal value of R_r. The motor is operating in motoring mode. When R_r^* is much larger than R_r, the pole P_2 is near the imaginary axis. The dynamic characteristic is influenced by R_r. Fig. 5 shows the root trajectories of the poles and zeros in which the motor is operating in regenerating mode. When R_r^* is much larger than $1.25R_r$, the pole P_1 is moved in an un-

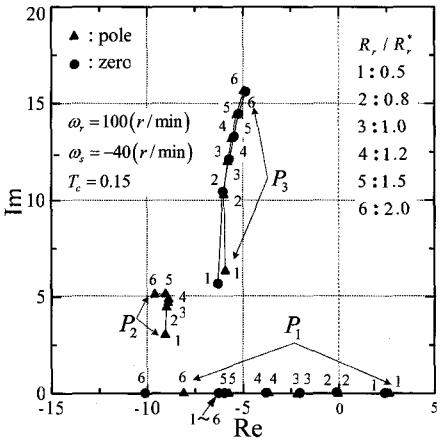

Fig. 5 Trajectories of poles and zeros with R_r change (In regenerating mode).

stable region. From this figure, we can know that R_r also has influence on system stability in low-speed regenerating operation, and its identification is important and necessary.

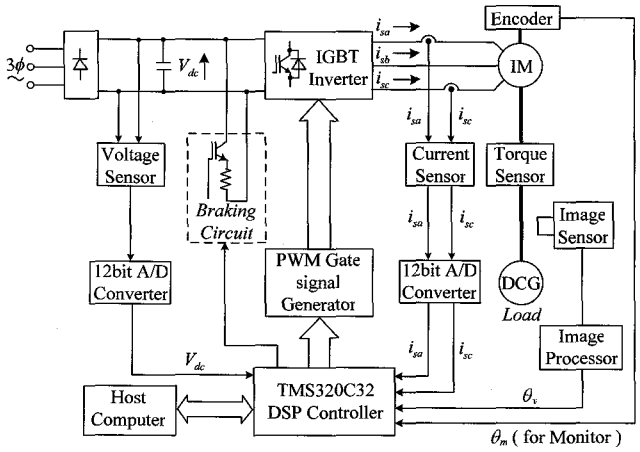

Fig. 6 Experimental configuration

4. Experimental Results

The proposed control system was implemented by a DSP (TMS320C32), as shown in Fig. 6. For speed control, two current sensors are used to detect the motor's phase currents and a voltage sensor is used to detect the dc link voltage of PWM inverter. The DSP controller receives the detected current signals and estimates the rotor speed for speed control and identifies the stator resistance. The position information from the speed sensor (Encoder) is sent to the DSP controller for computing the motor actual speed and checking the validity of the speed sensorless control system. The position information from the image processor is also sent to the DSP controller for calculating the motor speed and identifying the rotor resistance. The sampling or interrupting period is 200 μs. The electronic exposure period of the CCD camera used as the image sensor is 1/60 s. Fig. 7 shows the experimental setup.

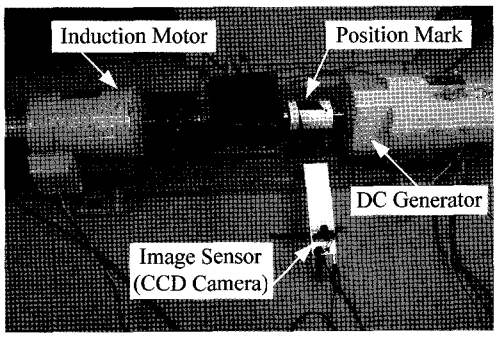

Fig. 7 Experimental setup

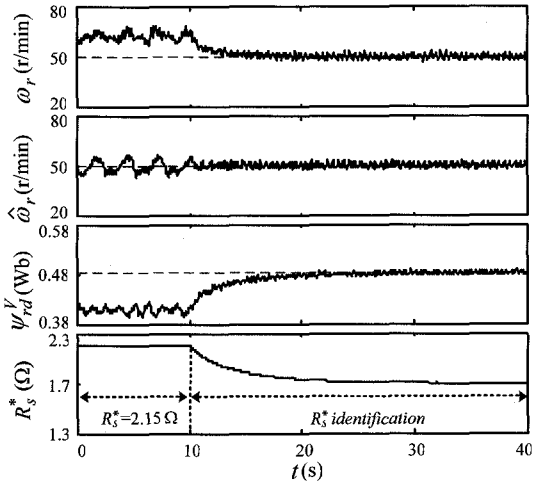

Fig. 8 Transient response of R_s identification

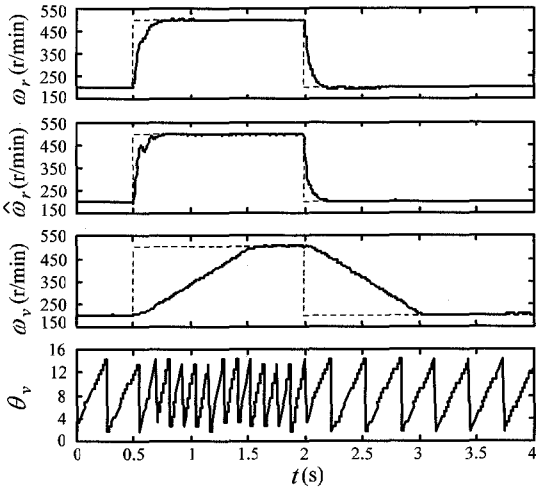

Fig. 9 Transient response of speed step change

4.1 Response of the Speed Sensorless Control System

The experimental results of the speed sensorless control system have been illustrated in [6]. The results of stator re-

sistance identification have also been presented in [6]. Here, we illustrate one of those results. Fig. 8 shows the experimental result of R_s identification at 50 r/min. The effectiveness of R_s identification is verified by this result.

Fig. 9 shows the experimental waveforms of the actual speed ω_r, the estimated speed $\hat{\omega}_r$, the calculated speed

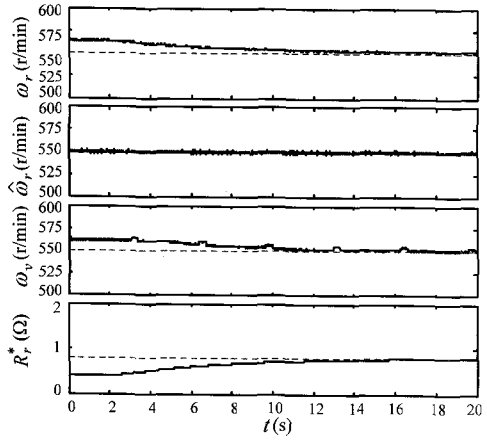

(a) $R_r^* < R_r$

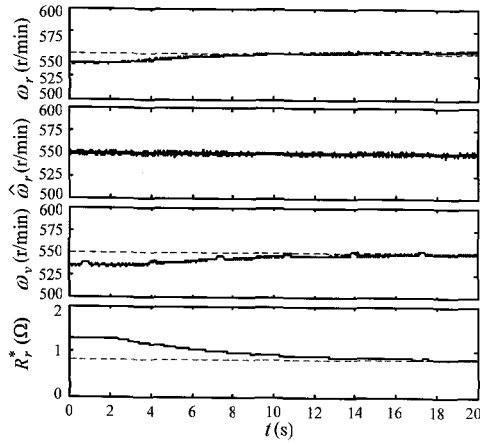

(b) $R_r^* > R_r$

Fig. 10 Transient response of R_r identification

ω_v, and the position value θ_v related to the motor axis mark by using the image processor when ω_r^* is changed form 200 to 500 r/min and then back to 200 r/min without load. The convergence time of ω_r is around 0.2 s. Because the ω_v calculation period T is set to be 1.0 s for improving calculation accuracy, the convergence time of ω_v is about 1.0 s. This result shows that ω_v can be used as the motor actual speed at a steady-state operation but cannot be used at a transient state. Because the electronic exposure period of the CCD camera is 1/60 s, the axis position is detected at every 1/60 s. ω_v can be correctly calculated only when the actual speed is below 1200 r/min.

4.2 Rotor Resistance Identification by Aid of Image Sensor

Fig. 10 shows the experimental results of R_r identification for $\mu_r = 4.0$ and $\omega_r^* = 550$ r/min. The motor is operating in regenerating mode and the load torque is -3.0 N·m. R_r identification begins at 2.0 s. In Fig. 10 (a), R_r^* is set to be 0.3935 Ω before R_r identification.

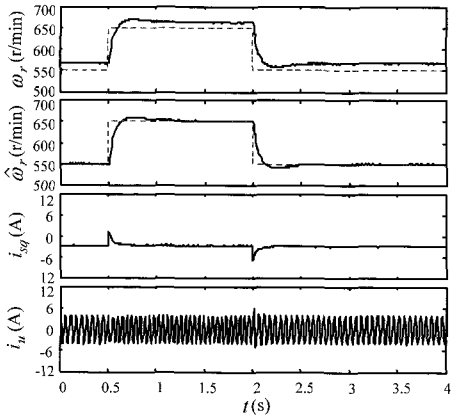

(a) $R_r^* < R_r$.

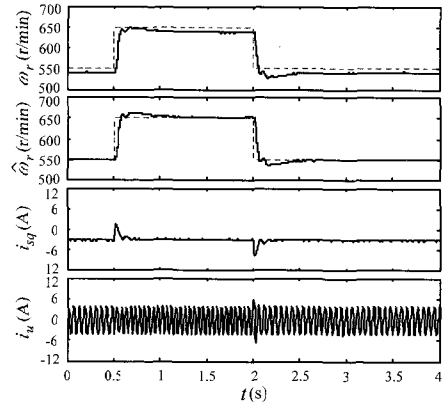

(b) $R_r^* > R_r$.

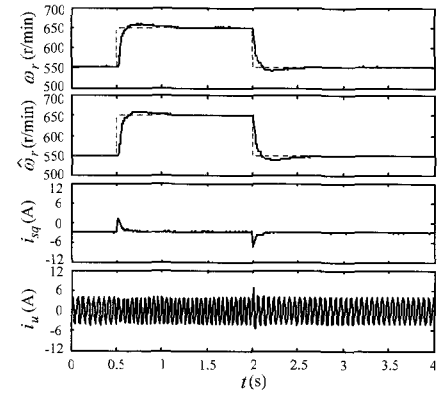

(c) After R_r identification.

Fig. 11 Transient response of speed step change with R_r influence

In Fig. 10 (b), R_r^* is set to be 1.3 Ω before R_r identification. Since the electronic exposure period of the CCD camera is 1/60 s, the ω_v value is changed at every 1/60 s. Therefore, the R_r identification gain must be set to be a small value for avoiding great variation of the motor actual speed and R_r is identified at every 1/60 s. The R_r identification time is around 16 s. Although $\hat{\omega}_r$ and ω_v shown in Fig. 10 have some ripples and there are little deflections of ω_r, ω_v and R_r^* after 16 s, the proposed R_r identification algorithm can be considered to work well in regenerating mode. In addition, even if there is an error between R_r and R_r^* before R_r identification, the estimated speed $\hat{\omega}_r$ is always converged to ω_r^* by PI speed regulator. But the actual speed ω_r is deviated from ω_r^* because of R_r error. With R_r identification, R_r^* is converged to a constant value and ω_r is converged to ω_r^*. This result shows that R_r identification is requisite for speed control accuracy. We are confident that the R_r identification algorithm using the image processor is valid in regenerating mode. And this algorithm can work in motoring mode also.

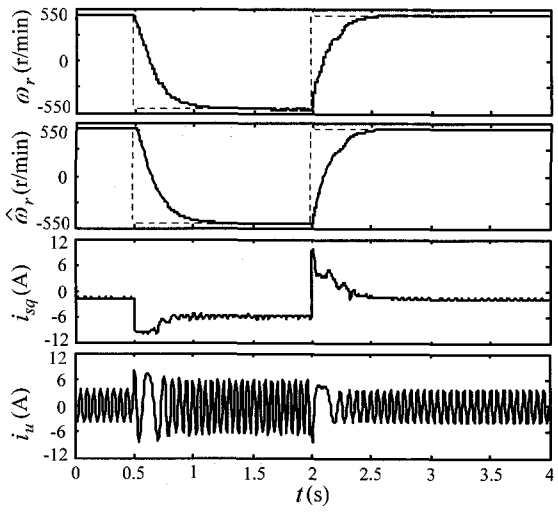

Fig. 12 Transient response of speed step change

Fig. 11 shows the experimental waveforms of ω_r, $\hat{\omega}_r$, the actual torque-producing current i_{sq}, and the u-phase current i_u while operating in regenerating mode. Here, the load torque is −3.0 N·m and ω_r^* is changed from 550 to 650 r/min and then back to 550 r/min. In Fig. 11 (a), R_r^* is set to be 0.3935 Ω. In Fig. 11 (b), R_r^* is set to be 1.3 Ω. Fig. 11 (c) shows the result after R_r identification. Because R_r^* is smaller than R_r, ω_r shown in Fig. 11 (a) is greater than $\hat{\omega}_r$ when operating at the steady state. In Fig. 11 (b), ω_r is smaller than $\hat{\omega}_r$ because of $R_r^* > R_r$. This reason can be explained by (14). After R_r identification, ω_r shown in Fig. 11 (c) is well converged to ω_r^* when operating at a steady state. This result shows that R_r identification is very important for high accuracy of speed control and the proposed image process is succeeded in improving the performance of vector-controlled induction motor system.

Fig. 12 shows the experimental waveforms of ω_r, $\hat{\omega}_r$, i_{sq}, and i_u. Here, ω_r^* is changed from 550 to -550 r/min and then back to 550 r/min. Operating at 550 r/min, the motor is in regenerating mode and the load torque is −2.0 N·m. Operating at -550 r/min, the motor is in motoring mode. The speed convergence time is around 0.5 s, the i_u phase reverses at the moment when $\hat{\omega}_r$ is 0. The four-quadrant operation and the speed zero crossing is stable.

5. Conclusions

In this paper, a mechanical sensorless vector-controlled system with the aid of image process for induction motor has been proposed. For high accuracy of speed and torque control, a rotor resistance identification algorithm was proposed by the aid of image processor. The following points summarize the work presented.

- Without mechanical sensor, the estimated flux based on the flux observer was used for speed estimation and stator resistance identification.
- Instead of a conventional mechanical sensor, the non-touched position detecting method using a small-size and low-cost CCD image sensor has been implemented.
- The estimated speed using flux error was used for speed control. The dynamic characteristic of the proposed system was only determined by the speed sensorless vector controller and not influenced by the low-performance image processor.
- According to the study of the linear model, rotor resistance has influenced on system stability in low-speed regenerating operation and its identification was important and necessary.
- With parameter identification, the performance of the proposed system has been greatly improved. And this system can do its work during both motoring and regenerating operations.

Appendix

Three-phase inductor motor parameters used for the experimental system

$R_s = 1.3\ \Omega$, $R_r = 0.787\ \Omega$, $L_s = 0.115$ H, $L_r = 0.115$ H, $M = 0.11$ H

rated output power	1.5 kW;
rated torque	8.38 N • m;
rated current	6.0 A;
rated rotational speed	1710 r/min;
pole number (P)	4;
moment of inertia(J)	0.0126 kg • m^2.

References

[1] D. Telford, M. W. Dunnigan, and B. W. Williams, "Online identification of induction machine electrical parameter for vector control loop tuning," *IEEE Trans. Ind. Electron.*, vol. 50, no 2. , April, 2003, pp. 253-261.

[2] T. Noguchi, S. Kondo, and I. Takahashi, "Field-orientated control of an induction motor with robust on-line tuning of its parameters," *IEEE Trans. Ind. Applicat.*, vol. 33, no. 1, Jan. /Feb., 1997, pp. 35-42.

[3] M. Tsuji, K. Tomonaga, M. Ohmachi, and K. IZUMI, "A novel parameter identification of vector controlled induction motor using a phase lag current control," in *Proc. IEEE IECON-2002*, November, 2002, pp. 329-334.

[4] C. Schauder, "Adaptive speed identification for vector control of induction motors without rotational transducers," *IEEE Trans. Ind. Applicat.*, vol. 28, no. 5, Sept. /Oct., 1992, pp. 1054-1061.

[5] P. Vas, *Sensorless Vector and Direct Torque Control,* Editor, London, U. K.: Oxford Univ. Press, 1998.

[6] M. Tsuji, S. Chen, K. Izumi, and E. Yamada, "A sensorless vector control system for induction motor using a-axis flux with stator resistance identification," *IEEE Trans. Ind. Electron.*, vol. 48, no. 1, Feb., 2001, pp. 185-194.

[7] P. C. Krause, *Analysis of Electric Machinery*, New York: McGraw-Hill, 1986.

[8] M. Tsuji, E. Yamada, K. Izumi, and J. Oyama, "Model following servo control of CSI-IM vector control system," in *Proc. IEEE IECON'91*, 1991, pp. 257-262.

Mineo Tsuji

He received the Ph.D. degree from Kyushu University, Japan, in 1981 in electrical engineering. He became a lecturer of Nagasaki University in 1981 and an associate professor in 1983. Since 2001 he has been a professor. His research interest is control of electrical machines and systems. He is a member of the IEEE and a senior member of IEE Japan. Dr. Tsuji received the Paper Award from the Institute of Electrical Engineers of Japan in 1998.

Shuo Chen

He received the B. S. degree from Nanjing University of Aeroautics and Astronautics, Chian, and the Ph. D. degree from Nagasaki University, Japan, in 1985 and 2000, respectively. He became a lecture at Fuzhou University, China, in 1994. Since 2003, he has been an assistant professor at Nagasaki University, Japan. His research interest are ac motor drives, control systems and mechatronics. Dr. Chen is a member of the IEEE and IEE Japan.

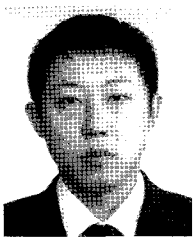

Tatsunori Motoo

He received the B. S. degree in electrical engineering from Nagasaki University, Japan, in 2004. And now, he is a graduate student for the M. S. degree in the same university. His research interests are in the areas of ac motor drives, namely, speed sensorless vector control of induction motor. He is a student member of IEE Japan.

Yuki Kawabe

He received the B. S. degree in electrical engineering from Nagasaki University, Japan, in 2005. And now, he is a graduate student for the M. S. degree in the same university. His research interests are in the areas of ac motor drives, especially speed sensorless vector control of induction motor. He is a student member of IEE Japan.

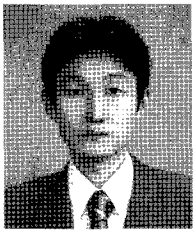

Shin-ichi Hamasaki

He received the B. S. and M. S. and Ph. D. degrees all in electrical engineering from Yokohama National University, Japan, in 1998, 2000 and 2003, respectively. Since 2003, he has been a research associate at Nagasaki University, Nagasaki, Japan. His research interests are in power electronics and digital control. He is a member of the IEEE and IEE Japan.